Master's thesis
Degree Programme in Atmospheric Sciences
Aerosol Physics

$PM_{2.5}$ and PM_{10} characterizations with a focus on Sand and Dust Storms episodes in the urban atmosphere in Amman, Jordan

Xinyang Li

May 2020

Supervisors: Prof. Tareq Hussein
Prof. Mar Viana*

Reviewers: Prof. Tuukka Petäjä
Prof. Veli-Matti Kerminen

UNIVERSITY OF HELSINKI

P.O.Box 64 (Gustaf Hällströmin katu 2)
FI-00014 University of Helsinki

* Institute of Environmental Assessment and Water Research (IDAEA-CSIC), C/ Jordi Girona 18, 08034 Barcelona, Spain

Tiedekunta — Fakultet — Faculty	Koulutusohjelma — Utbildningsprogram — Education programme
Faculty of Science	Master's Programme in Atmospheric Sciences

Tekijä — Författare — Author

Xinyang Li

Työn nimi — Arbetets titel — Title

Master student

Opintosuunta — Studieinriktning — Study track

Aerosol physics

Työn laji — Arbetets art — Level	Aika — Datum — Month and year	Sivumäärä — Sidoantal — Number of pages
Master's thesis	May, 2020	34 pages

Tiivistelmä — Referat — Abstract

The impacts of dust aerosols on human health and climate change are increasing as the particulate matter (PM) mass concentrations and frequency of Sand and Dust Storm (SDS) episodes have shown an increasing trend in recent studies, especially for the Middle East and North Africa (MENA). In this thesis, particulate matter (PM_{10} and $PM_{2.5}$) concentrations were measured during May 2018–March 2019 in the urban atmosphere of Amman, Jordan. The PM sampling was 24-hours every 6 days. The overall mean PM_{10} mass concentration was 64±39 μg/m^3 with the median (+interquartile range) value of 49.2+53.5 μg/m^3, the $PM_{2.5}$ mass concentration varied between 15 μg/m^3 and 190 μg/m^3 with an annual average 47±32 μg/m^3 and with the median (+interquartile range) value of 35.8+26.3 μg/m^3. The $PM_{2.5}$ / PM_{10} ratio was 0.8±0.2. According to the Jordanian Air Quality standards, the annual mean PM_{10} needs to be below a limit value of 120 μg/m^3, which was true in this work. However, the $PM_{2.5}$ mass concentration was three times higher the corresponding limit value (65 μg/m^3). However, both exceeded the World Health Organization (WHO) air quality annual guideline of 20 μg/m^3 for PM_{10} and 10 μg/m^3 for $PM_{2.5}$. The results show that the observed PM_{10} mass concentrations in Jordan were lower than what was reported in other cities in the Middle East but were higher when compared to other Mediterranean cities. During the measurement period, Jordan was affected by Sand and Dust Storms (SDS), which were observed on 14 sampling days. The source origins of these SDS were traced back to North Africa, the Arabian Peninsula, and the Levant. The 24-hour PM_{10} concentrations during these SDS episodes ranged between 108.1 μg/m^3 and 187.3 μg/m^3. In the future, measurements with a higher time resolution (one sample per day) are recommended for a more precise seasonal trend interpretation.

Avainsanat — Nyckelord — Keywords

urban air quality; particulate matter; dust particles; back-trajectory; dust origins; measurement.

Säilytyspaikka — Förvaringsställe — Where deposited

E-thesis University of Helsinki

Muita tietoja — övriga uppgifter — Additional information

Contents

1. Introduction

Aerosols are airborne solid or liquid fine particles suspended in a carrier gas (Hinds, 1999, p. 3). Owing to their physical and chemical characteristics, the increasing amount of scientific literature has revealed their adverse health effects and significant impacts on the environment and climate (e.g. Aitken, 1880; Maring, H. et al., 2003; Pope and Dockery, 2006; Alonso-Pérez, S. et al., 2007; IPCC, 2007; West J. J. et al., 2013; Apte J. S. et al., 2015; Latif M. T. et al., 2018; Mbengue, S. et al., 2020). The particulate aerosols, such as $PM_{2.5}$ (particles with aerodynamic diameter smaller than or equal to 2.5 μm) and PM_{10} (particles with aerodynamic diameter smaller than or equal to 10 μm), are small enough to enter human respiratory system via inhalation and trigger potential health impacts. Cardiovascular and respiratory problems have been associated with long-term exposure and inhalation of particulate matter, which include dust particles (Pope et al., 2002; Hoek et al., 2013). Aerosols also directly and indirectly affect the Earth's atmosphere and further influence the behavior of the ecosystem (e.g. Mencuccini and Grace, 1995; Morales-Baquero1 et al., 2006; Swann et al., 2010; Zou et al., 2020).

In urban areas, the origins of aerosols are from a vast range of local natural and anthropogenic sources and long-distance transportation by air masses. As sources of one specific type of aerosol, dust storms occur mostly at arid and semi-arid areas where there is sufficient amount of dust particles (e.g. desert) and atmospheric wind with enough strength to move the dust particles (Bagnold 1941, Kok et al. 2012, Middleton 2017). The Eastern Mediterranean region suffers from increasing amount of Sand and Dust Storm (SDS) episodes, which have been reported more frequently during the past decades (UNEP, 2001; Kutiel et al, 2003; Amarloei et al, 2019; Abdullah et al, 2019; Saeifar et al, 2019). For climate impacts, Notaro et al. (2015) confirmed a dust episodes regime shift from inactive before 2006 to active during 2007-2013 in Arabian Peninsula emphasizing the significance of investigating SDS episodes and origins. Considering such change and the increasing SDS frequency in Middle East, higher surface reflection due to increasing albedo in the atmosphere was observed (Satheesh et al. 2006), which led to the Earth surface temperature decrease with continuous impacts.

In general, SDS episodes occur via three modes: saltation, creep, and suspension (e.g. d'Almeida et al. 1974, Shao et al.1993). During SDS episodes, dust particles are susceptible to turbulent fluctuations and can remain airborne for a short-term (diameter 20–70 μm) or long-term (diameter < 20 μm) (e.g. Natsagdorj et al. 2003, Kok et al.2012, Evan et al. 2016). Short-term suspended dust has a local effect whereas long-term suspended dust stays airborne up to several weeks and can be transported for thousands of kilometers from its source region (e.g. Gillette and Walker 1977, Zender et al.2003, Miller et al. 2006, Kok et al. 2012, Zoljoodi et al. 2013, Doronzo et al. 2015, Gherboudj et al. 2017).

Most of the dominant sources of natural dust aerosols are in the arid and semi-arid areas in the northern sphere (e.g. Middleton 1986a and 1986b, Prospero et al. 2002, Goudie 2009, Cao et al., 2015). Recently, Gherboudj et al. (2017) characterized the spatiotemporal variability of the Middle East and North African Dust Emission Potential (MENA-DEP) according to three scales: low dust emission areas, moderate dust emission areas, and high dust emission areas. It had

classified that in the Middle East, the high and moderate dust emission areas were Jordan, Syria, east Iraq, and Arabian Peninsula. In addition to these areas, central Iran, west Afghanistan, south-west Pakistan, and west India belong to the low dust emission areas.

The dust source areas in the Levant, Arabian Peninsula, and Iran were also identified and investigated in several previous studies (e.g. Rezazadeh et al. 2013, Alam et al. 2014, Cao et al. 2015, Nabavi et al. 2016, Rashki et al. 2017). Among these locations, the SDS event frequencies Arabian Peninsula has so far been the highest (Jish Prakash et al., 2015).

The Eastern Mediterranean region suffers from Sand and Dust Storm (SDS) episodes, which have been reported more frequently during the past decades (UNEP, 2001; UNDP 2002; Kutiel et al. 2003; Keramat et al. 2011; Hamidi et al. 2013; Amarloei et al, 2019; Abdullah et al, 2019; Saeifar et al, 2019). The increased frequency of SDS in the Eastern Mediterranean region has been ascribed to the impact of climate change and its consequences by desertification, deforestation, wetland destruction, increased population growth and anthropogenic emissions, food insecurity, and water shortage (e.g. Amiraslani and Dragovich 2011; Rezazadeh et al. 2013; Notaro et al. 2015). Notaro et al. (2015) showed that the Eastern Mediterranean region has suffered of warming and drying episodes since the beginning of this century. This led to an increased potential to collapse the Fertile Crescent (namely Iraq and Syria). Furthermore, the Arabian Peninsula has experienced pronounced interannual to decadal variability in dust activity with an abrupt regime shift in 2006 from an inactive dust period during 1998–2005 to an active dust period during 2007–2013. Notaro et al. (2015) further recalled the onset of this regime shift to the climate state transitioned into a combined La Niña and negative phase of the Pacific Decadal Oscillation, which incited a hiatus in global warming in the 2000s. As such, a devastating and prolonged drought engulfed the Fertile Crescent and led to crop failure. In turn, the dried soils and diminished vegetation cover in the Fertile Crescent, which was evident through remotely-sensed enhanced vegetation indices, supported greater dust generation and transport in the Middle East during 2007–2013. The increased dust episodes and atmospheric dust concentrations on top of the atmosphere have a significant impact on the albedo and short-wave radiation over the Middle East leading to higher surface reflection (Satheesh et al. 2006).

Besides climate change impacts, the increasing concentrations of anthropogenic aerosols during the previous decades in the Middle East have other plausible effects (e.g. Givati & Rosenfeld 2007). These particles are anticipated to slow down the conversion of cloud drops into raindrops and snowflakes, thus decreasing precipitation from short-lived clouds such as those formed in moist air that crosses topographic barriers. This, in turn, escalated the desertification process in the Middle East, causing increased frequency of dust episodes and atmospheric dust particle concentrations.

While aerosol research has been given increased attention in the Eastern Mediterranean, it is still at an early stage in the Middle East (e.g. Ahmad et al, 2019), especially in Jordan (e.g. Hussein et al. 2018). Therefore, this work aims at investigating the particulate matter (PM_{10} and $PM_{2.5}$) concentrations over a measurement period between May 2018 and March 2019 in the urban atmosphere of Amman, Jordan. The methods included aerosols sampling using high volume

samplers and gravimetric analysis combined with air mass back trajectories to identify the source origin of SDS episodes.

2. Materials and methods

2.1. Measurement location

The long-term aerosol measurement campaign was performed during May 2018 – March 2019 on the roof top (about 20 m above the ground) of the Department of Physics at the campus of the University of Jordan [32.0129N,35.8738E]. The campus is situated at an urban background location in the northern part of Amman, which is the capital city of Jordan. The surrounding area of the campus is a mixture of residential area and road network with one of the main roads (Queen Rania street) passing parallel to the west side of the campus (Figure 1). The downtown was about 10 km south of the campus area.

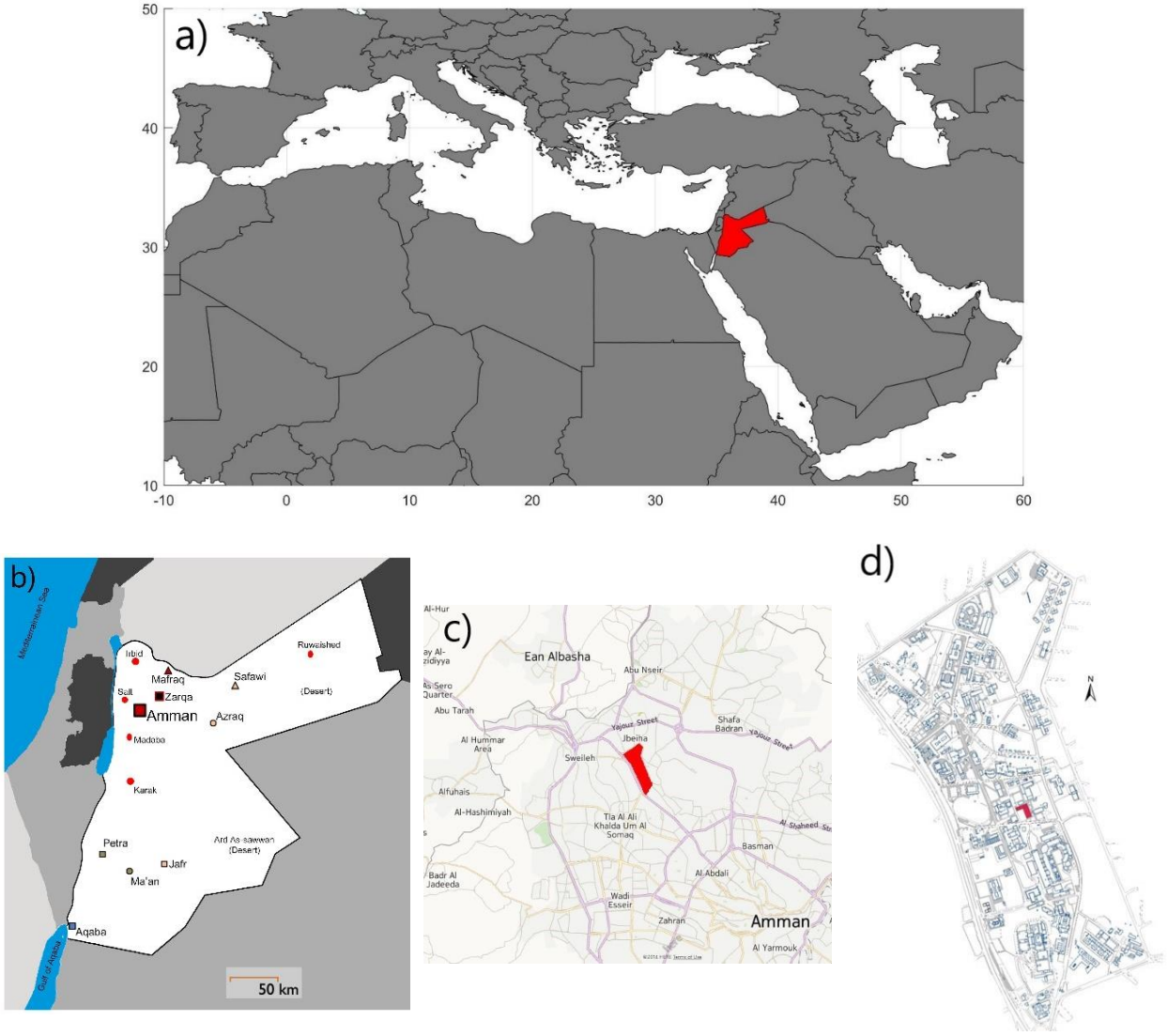

Figure 1: Maps showing (a) the Mediterranean Sea region with Jordan highlighted in red, (b) Jordan with highlights on the geographical locations of main cities, (c) road network and the campus of the University of Jordan (red shaded area) inside Amman, and (d) details of the campus of the University of Jordan with the sampling location (red shaded area) at the middle of the campus.

2.2. Aerosol measurements

2.2.1. High volume sampling

Two high-volume samplers (model CAV-A/mb, MCV, S.A., Spain) were used for $PM_{2.5}$ and PM_{10} by setting the cascade impactors (model PM1025-CAV, MCV, S.A.) aerodynamic diameter to be lower than 2.5 µm and 10 µm, separately. A demonstration of an entire measurement equipment is illustrated in Figure 2. The high-volume samplers were operated at 30 m^3/h flowrate and recorded the temperature and pressure during all the sampling session. These cascade impactors can accommodate one 15-centimetre diameter round filter, which in this work were quartz fibre filters (Pallflex, PALLXQ250ETDS0150, TISSUQUARTZ 2500 QAT-UP).

Each sampling session measured PM_{10} and $PM_{2.5}$ mass for 24-hours with a time resolution of 6 days. There were in total 48 $PM_{2.5}$ samples 51 and PM_{10} samples including all blank samples. The blank samples were taken once for $PM_{2.5}$ sampling and 3 times for PM_{10} sampling during the campaign by following the same procedure as for the active sampling except that the high-volume sampler was turned off (i.e. zero flow rate). The blank samples were necessary for the accuracy check of the sampling procedure and analysis (Querol et al, 2004).

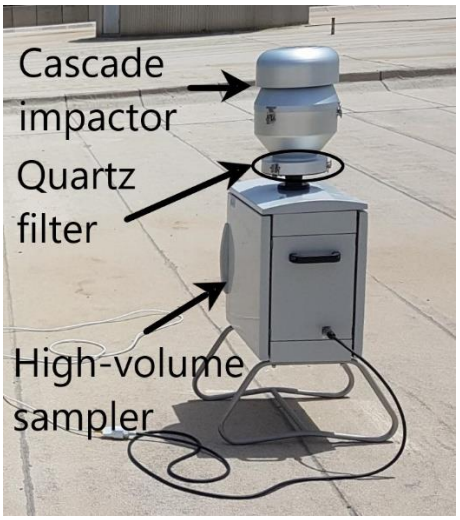

Figure 2: High-volume sampler with cascade impactor on the top.

2.2.2. Gravimetric analysis

The air filter samples were stored in freezers in the Department of Chemistry building in University of Jordan once every measurement session was complete. The gravimetric analysis was processed according to the European directive EN1234-1 (20 ºC and 50% RH) at the Institute of Environmental Assessment and Water Research (IDAEA-CSIC, Barcelona, Spain) after the transportation of air samples (with cooling packs) from Amman to Barcelona. The gravimetric analysis included pre-sampling and post-sampling weighing of each filter (including blanks). The pre-weighing and post-weighing were done with the same procedure: conditioning temperature 20 ºC and relative humidity (RH) 50%. The conditioning time was 2 days. Each sample was weighed twice (24 hours interval in between) and the average value was recorded (Figure 3 right). The weighing was made using a microbalance (Mettler-Toledo, model: XP105 with electrostatic charge detection, Switzerland) shown in Figure 3 (left).

The 24-hour average particulate matter concentration (PM_x [µg/m^3]) was calculated

$$PM_x = \frac{m_{post} - m_{pre}}{Q \times \Delta t} \quad (1)$$

where m_{post} and m_{post} [µg] are the post sampling and the pre-sampling weight of the filter, Q [30 m^3/h] is the sampling flow rate, and Δt [24 hours] is the sampling time interval.

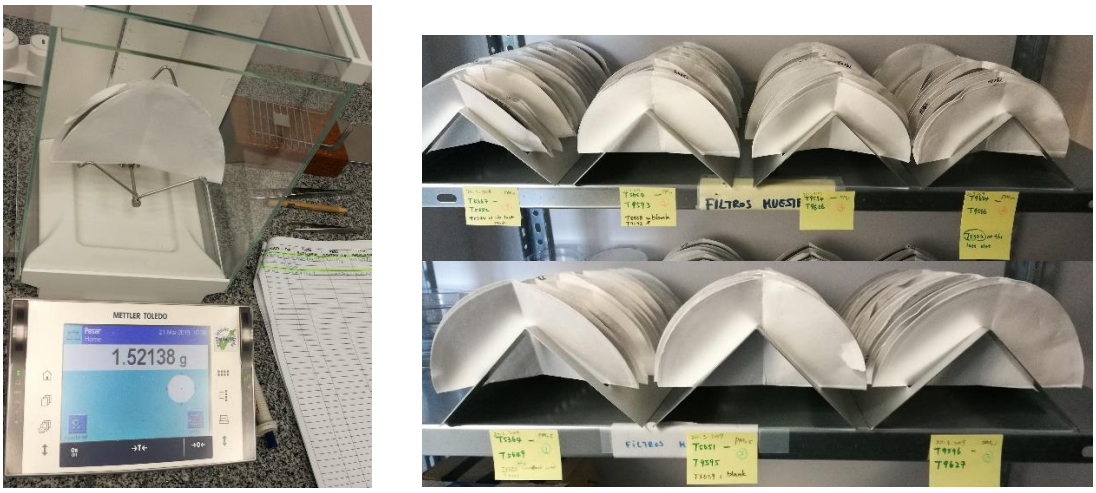

Figure 3: Sample weighing using microbalance (left) and sample conditioning under stable environmental conditions of 20 °C and 50% RH (right).

2.3. Supporting data

2.3.1. Meteorological conditions

The weather conditions were monitored on-site with a weather station (WH-1080, Clas Ohlson: Art.no. 36-3242), which was set to record the reading with five minutes interval. The weather data consisted of ambient temperature (−40–65 °C, resolution 0.1 °C), barometric pressure (918.7–1079.9 hPa, resolution 0.3 hPa), relative humidity (10%–99%, resolution 1%), wind speed (1–160 km/h) and direction (divided into 16 wind sectors), and precipitation (0–9999 mm, resolution 0.3 mm below 1000 mm and 1 mm over 1000 mm).

The weather conditions were observed for the rain episodes accompanied with low PM_x ($PM_{2.5}$, PM_{10}) for clean days analysis.

2.3.2. Back trajectory model

Air mass back-trajectories were calculated using the HYSPLIT model (e.g. Draxler and Hess, 1997; Draxler and Rolph 2012; Stein et al., 2015), which provides detailed information about the origin and path of air masses that arrived at the measurement site. Four-days isentropic back trajectories were calculated for each hour at the arrival heights of 100, 500 and 1500 meters.

The back trajectories crossing maps were generated in terms of the frequency of air mass crossing over each grid cell of the domain. The domain was taken to cover the west-south Asia, North Africa, and Europe (i.e. longitude -20°–60° and latitude 15°–55°). The crossing map resolution was set to 0.5° for the 4-day back trajectories calculated for each hour.

3. Results and Discussion

3.1. Meteorological conditions and air mass back-trajectories

3.1.1. Meteorological conditions

The hourly, daily, and monthly means of the meteorological parameters (ambient temperature (T), relative humidity (RH), absolute pressure (P), wind speed (WS), and hourly precipitation) are presented in Figure 4. The monthly mean, standard deviation, minimum, and maximum values are listed in Appendix 1.

The ambient temperature (T) showed a clear seasonal variation with high values during summer (June–August, monthly mean 24 ℃) and low values during winter (December–February, monthly mean 9). The daily mean T was in the range of 3–30 ℃ (overall mean 17±7 ℃) within the whole measurement period (Figure 4a).

Within the measurement period, May 2018 – March 2019, the daily mean RH (Figure 4b) was in the range 20–100 %. The lower RH mostly occurred in summer and autumn, while it was higher in winter and spring as precipitation increased.

For the absolute pressure, the daily mean P (Figure 4c) was in the range 890–908 hPa. The trend showed lower P in summer and autumn, higher P but more fluctuation pattern in winter and spring.

The wind speed (WS) showed a different monthly variation than T, RH, and P. The monthly mean WS was minimum during the autumn (September – November) and maximum during the summer (Figure 4d). During May 2018 – March 2019, the maximum daily mean WS was about 3.6 m/s.

The records of the accumulative rainfall represented a clear seasonality in that the precipitation in summer and autumn was very low (i.e. May-December 2018, cumulative ~50 mm) (Figure 4e), which was then followed by major (from 50 mm to 470 mm) precipitation episodes: the first one in the beginning of December 2018, the second one in mid-December 2018, and the third one in the beginning of March 2019. The rain accumulated intermittently in-between the mid-December 2018 and the beginning of March 2019. This phenomenon provided great potential of wet deposition of the dust particle, which could be observed in the PM mass concentrations.

The high-volume sampler recorded the 24-hour mean temperature (T) and pressure (P) during sampling sessions. These data are consistent with the weather station measurements (Appendix 2, Figure 5), and are therefore not shown in the main text. The correlation coefficient r was 0.99 and 0.97 for T and P, respectively. Hence, the overall measurement from the high-volume sampler was reliable based on the data consistency.

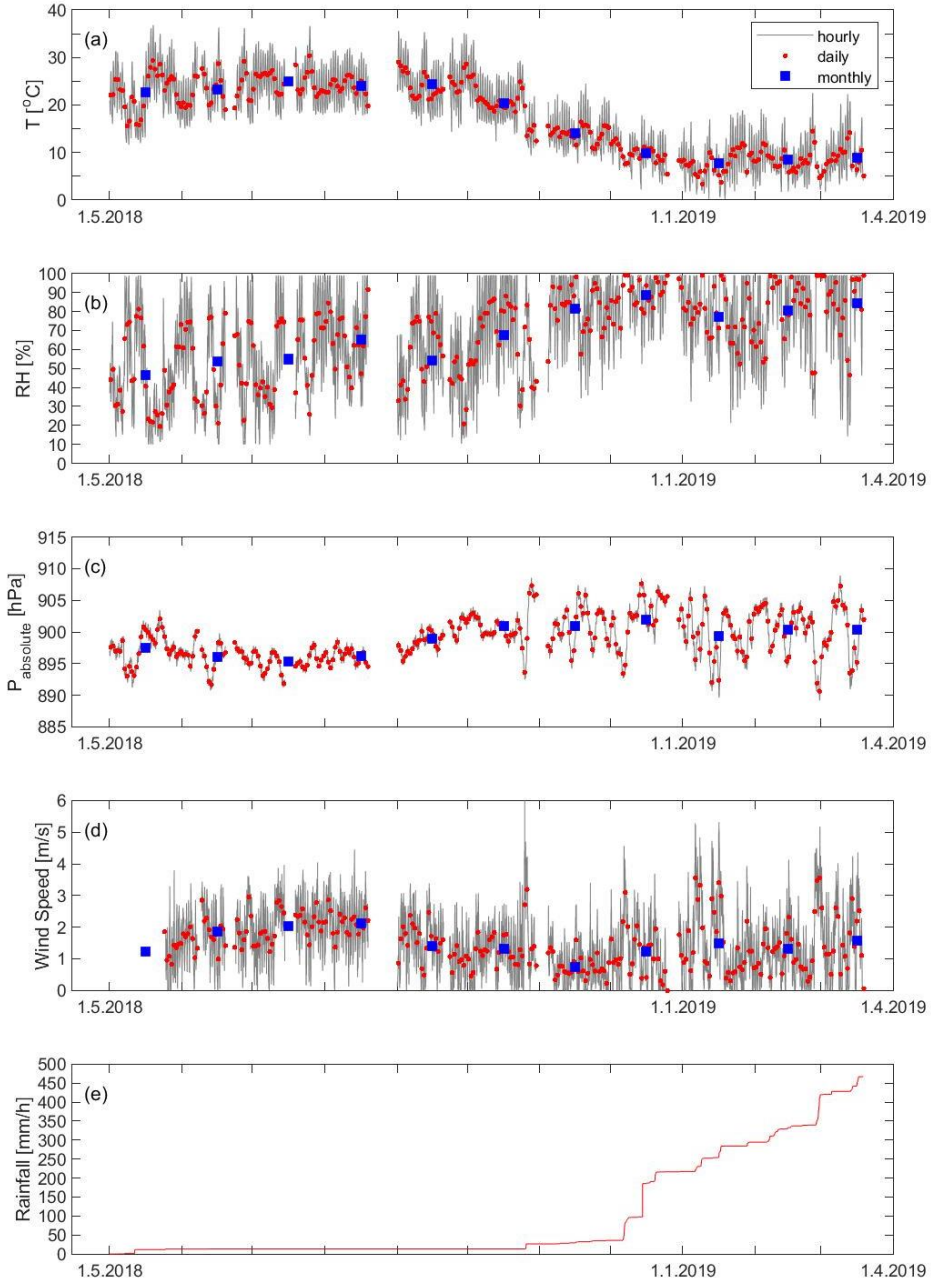

Figure 4. Time series of weather conditions during May 1, 2018 – March 19, 2019 presented as hourly, daily, and monthly means for (a) ambient temperature, (b) relative humidity, (c) absolute pressure, and (d) wind speed. (e) The rainfall was presented as hourly cumulative precipitation.

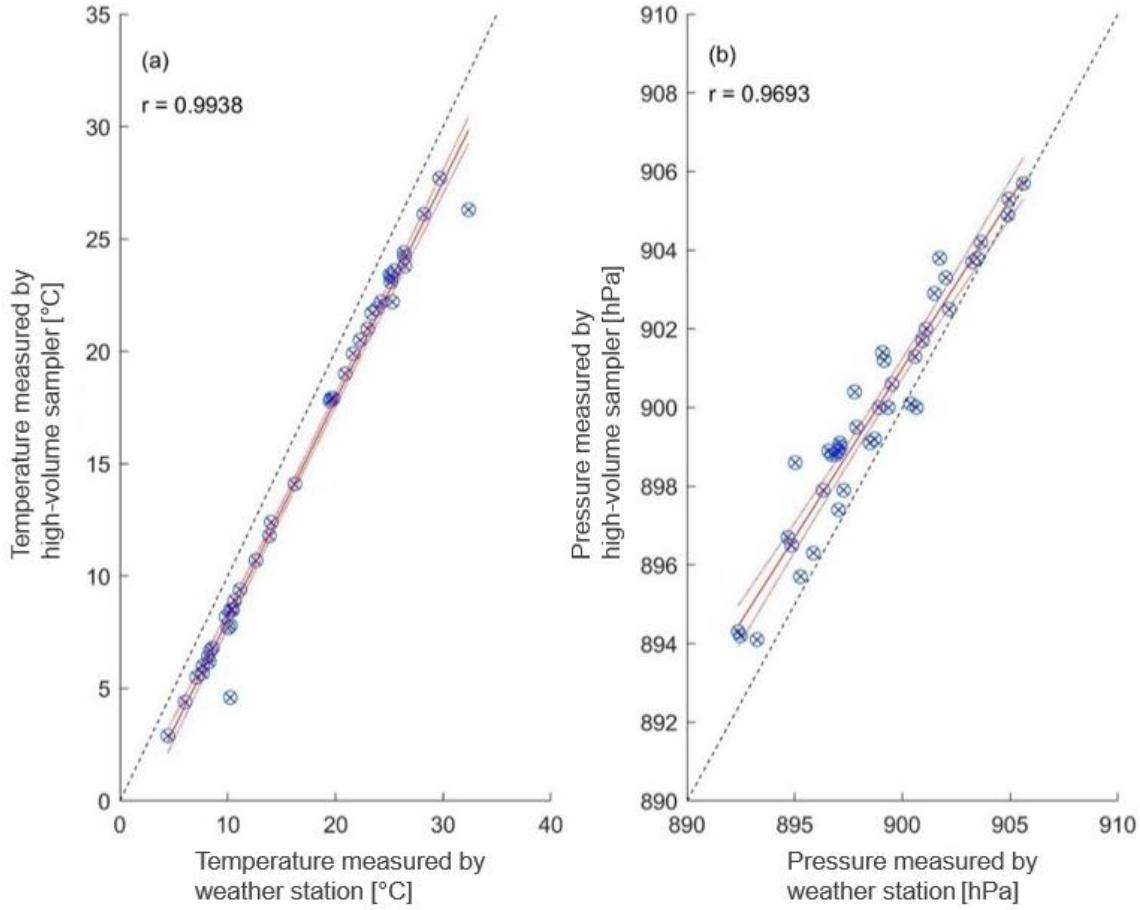

Figure 5. Temperature and pressure measurements comparison between the high-volume sampler and the weather station during the sampling sessions. The black dashed line represents the 1:1 line.

3.1.2. Air mass back-trajectories

The 4-day back trajectories crossing maps are presented in Figure 6 for the arrival heights of 100 m and 1500 m. The spatial extent of the trajectories crossing for the 1500 m arrival height was broader than that for the 100 m arrival height. For back trajectories arriving at the 1500 m height, they covered the whole Mediterranean Sea Basin and included north Africa, Red Sea, north and middle region of the Arabia Peninsula, the Levant with an extension to the Caspian Sea, and Europe. As for the arrival height of 100 m, the back trajectories covered the middle and eastern parts of the Mediterranean Sea, northeast Africa, north Red Sea, north Arabian Peninsula, the Levant, and southeast Europe. Furthermore, trajectories arriving at 100 m showed a predominant crossing path tracked back along the Eastern Mediterranean region: (1) it started from the Bosporus (Strait of Istanbul), which connects the Black Sea with Sea of Marmara, and the Aegean Sea, (2) crossing over the Eastern Mediterranean Sea between Crete and Cyprus before reaching Amman.

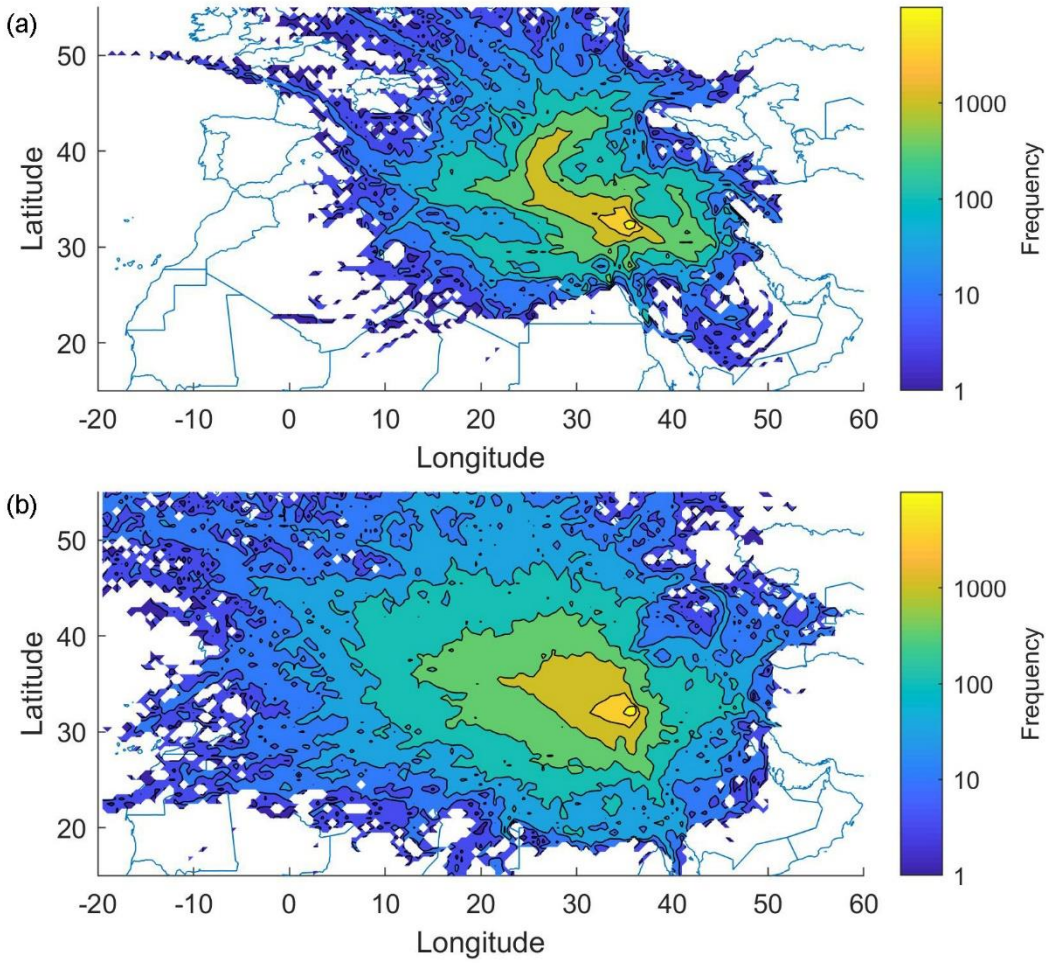

Figure 6. Back trajectories (96 hours) crossing maps at the arrival heights of (a) 100 meters and (b) 1500 meters. The arrival location was the campus of the University of Jordan, Amman, Jordan. These maps were generated from the hourly trajectories during May 1, 2018 – March 31, 2019.

3.2. Particulate matter (PM) mass concentration trend

Throughout the measurement period (Figure 7a and Appendix 2), the PM_{10} daily concentration varied between 20 µg/m^3 and 190 µg/m^3 with an overall average (± standard deviation) of 64±39 µg/m^3, and with the median (+interquartile range) value of 49.2+53.5 µg/m^3. The $PM_{2.5}$ daily concentration varied between 15 µg/m^3 and 190 µg/m^3 with an annual average 47±32 µg/m^3 and with the median (+interquartile range) value of 35.8+26.3 µg/m^3. The overall mean value of $PM_{2.5}$ / PM_{10} ratio was 0.76±0.2; i.e. 76.5% of the PM_{10} was within the fine fraction (Figure 7b and Appendix 2). Hussein (2017) reported the PM_{10} mass concentration from a similar measurement at the same site to be 3.7 – 126.4 µg/m^3 during the Springtime (March and April 2014), and the values were calculated using particle size distribution data. In contrast, during the study period in this work, the PM_{10} mass concentration was significantly higher (61.9 – 192.6 µg/m^3 in March 2019).

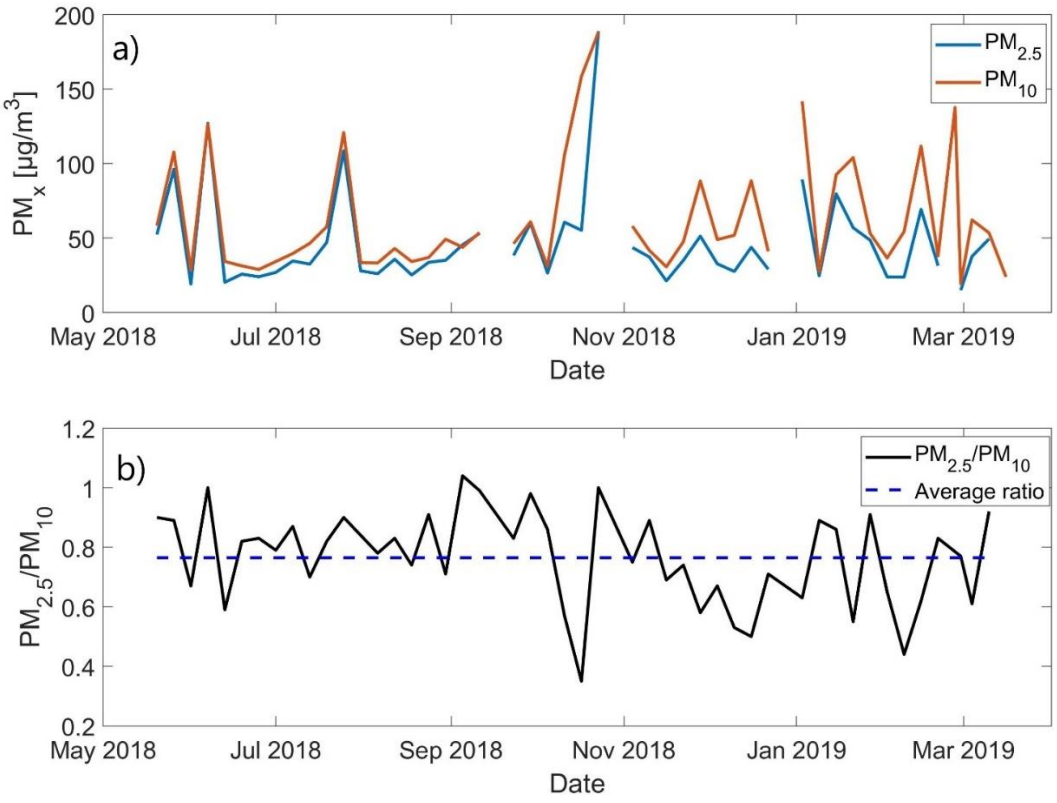

Figure 7. a) Time series of the measured 24h mean $PM_{2.5}$ and PM_{10} concentrations. b) $PM_{2.5}$ concentration ratio in PM_{10} (black solid line) with the average ratio of 0.765 (blue dash line).

The PM concentrations did not show a clear seasonal variation, which was different from the observation from the measurement between November 2013 to July 2017 that low PM mass concentration appeared more frequently in summertime, while high PM mass concentration occurred in wintertime (Hussein et al., 2018). PM_x mass concentrations exceeding the limit values could be seen in all the seasons. This phenomenon was opposite to the previous observations reported via on-line, continuous, long-term measurements of the particle number size distribution (e,g, Hussein et al., 2018, Hussein et al., 2019). The discrepancy between the 2013-2017 data and the results obtained in this work are probably an artefact resulting from the low temporal resolution of the 2018-2019 data. For instance, air mass back-trajectories were generated every day during the measurement period (2018-2019), and the observations in May and June 2018 showed the high frequency of air mass coming from MENA region before and after the measurement days. However, this indication of high PM mass concentration due to large air mass transportation was not evidenced because of measurement time resolution of 6 days. Therefore, doing the sampling with a higher time resolution is recommended (i.e. one sample per day if possible).

Among the $PM_{2.5}/PM_{10}$ mass concentration ratio, there were 4 measurements recorded the $PM_{2.5}/PM_{10}$ concentration ratio had exceeded 100%, which in principle seemed like an abnormal case. The results from ion chromatography analysis showed an overall higher ammonia ion concentration (NH_4^+ [ppm]) on the filters for the dates when $PM_{2.5}/PM_{10}$ concentration ratio was larger than 100%. The current hypothesis for these cases could be that the NH_4^+ concentration has an impact on PM_{10} mass concentrations owing to the sea salt content in the total sample mass, by means of an artefact already reported in the literature (Harrison & Pio, 1983, Warneck, P, 1988,

Harrison & Kito 1990). The sea salt particles are coarse and therefore are mostly collected on PM_{10} filters, and not on $PM_{2.5}$ ones. On the PM_{10} filters, the sea salt aerosols react with particulate NH_4NO_3 resulting in particulate $NaNO_3$ and volatile NH_4Cl, which is lost from the filter. This artefact results in artificially low PM_{10} mass concentrations, which on the dates when it was detected resembled PM2.5 concentrations. This is expected to have resulted in the observed $PM_{2.5}/PM_{10}$ ratios >1. The influence of this artefact has been reported in studies in the Mediterranean region (Viana et al. 2006, 2007; Putaud et al., 2009).

According to the Jordanian standards (JS 1140, 2006) for ambient air quality, the annual mean the PM_{10} and $PM_{2.5}$ must not exceed 70 µg/m^3 and 15 µg/m^3; respectively. However, the observed PM_{10} annual mean value was below the annual limit, whereas the $PM_{2.5}$ annual mean was three times higher than the limit. For the 24h mean limit value, PM_{10} and $PM_{2.5}$ must not exceed 120 µg/m^3 and 65 µg/m^3, respectively. However, the PM_{10} mass concentrations exceeded the limit for 6 times and $PM_{2.5}$ for 7 times. All the exceedance cases were observed during the reported Sand and Dust Storm (SDS) episodes in section 3.3. Compared to the World Health Organization (WHO) air quality guidelines for PM_{10} (annual and 24h must not exceed 20 µg/m^3 and 50 µg/m^3; respectively) and $PM_{2.5}$ (annual and 24h must not exceed 10 µg/m^3 and 25 µg/m^3; respectively), the observed annual concentrations here are exceeded both annual limit values. By aligning with the 24h WHO guideline, only 6 days did not exceed the $PM_{2.5}$ limit value 25 days did not exceed the PM_{10} limit value.

The WHO (2018) released an update for the global ambient air quality database that reported the annual mean PM_{10} and $PM_{2.5}$ concentrations during 2008–2016. Recalling the data for three Jordanian cities (Al-Zarqa', Amman, and Irbid) in 2017, the annual mean PM_{10} was 82, 68, and 53 µg/m^3; respectively. These observations are consistent with the annual mean PM_{10} ~64 µg/m^3 observed here. The world overall annual mean PM_{10} was ~72 µg/m^3 during 2008–2016, which is slightly higher than what we observed during our measurement campaign.

In general, the annual mean PM_{10} concentrations in Jordan were higher than what was reported by the WHO (2018) in urban, suburban, and residential sites in countries around the Mediterranean Sea in 2016. For example, the annual mean PM_{10} was 52±18 µg/m^3 (range 17–91 µg/m^3) for Turkish cities (80 sites), 25±6 µg/m^3 (range 10–43 µg/m^3) for Italian cities (231 sites), 52±18 µg/m^3 (range 21–43 µg/m^3) for Greek cities (12 sites), 37±6 µg/m^3 (range 29–41 µg/m^3) for Cypriot cities (4 sites) and 38±8 µg/m^3 (range 32–43 µg/m^3) for wo Maltese cities.

Compared to other cities in the Middle East as reported by the WHO (2018), the annual mean PM_{10} concentrations in Jordan were lower than what was observed in Kuwait (130±35 µg/m^3; 9 sites), Israel (90 µg/m^3), Egypt (249–284 µg/m^3; two sites), and the United Arab of Emirates (122–153 µg/m^3; three sites).

3.3. Sand and Dust Storm (SDS) episodes

As indicated in Figure 8, the days with PM_{10} concentrations higher than 70 µg/m^3 were considered as Sand and Dust Storm (SDS) episodes (Appendix 4). In practice, this threshold is slightly higher than the annual PM_{10} mean value. Based on this threshold, 14 days of SDS episode observations were obtained as listed in Appendix 3. According to the air mass back trajectories analysis, the

atmospheric SDS was transported from three main source regions: (1) long-range transport from north Africa (Sahara), (2) medium range transport from the Arabian Peninsula, and (3) short-range transported from the Levant. In some cases, the transport was a combination of two or three regions. Accordingly, three different air mass transport types were defined: S-type originated from Sahara region, SL-type originated from Sahara region and the Levant region (i.e. SDS combined from these two regions), and SLA-type originated from all three regions. The SLA-type was the most common SDS type because the back trajectories originated from north Africa crosses or circulates over the northern part of the Arabian Peninsula and the Levant region.

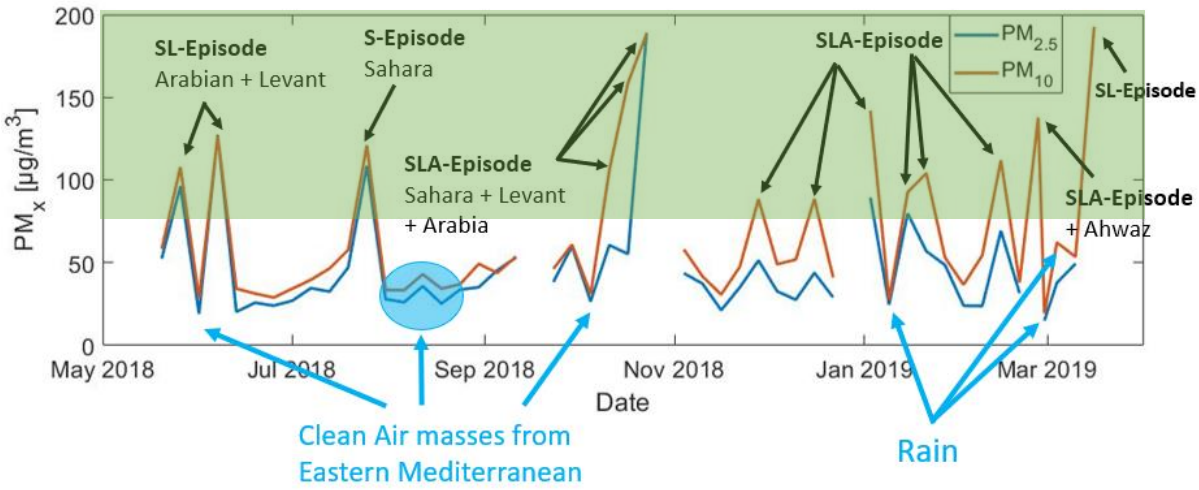

Figure 8. Time series of PM_{10} concentrations with markups for sand and dust episodes (SDS) and clean air periods (i.e. PM_{10} concentrations < 50 µg/m^3). The green-shaded area is the range of PM_x mass concentrations in which the SDS episodes were identified mostly based on PM_{10} exceedances.

During the measurement period, a single S-type SDS episode was identified on the 25th July 2018 with the PM_{10} of 121.9 µg/m^3 and PM2.5 of 108.4 µg/m^3, which was solely originated from the Sahara region (Figure 9). Interestingly, during this episode the back trajectories arriving at 1500 m (Figure 9c) originated from and crossed over North Africa, whereas those arriving at 100 m and 500 m (Figure 9a–b) were from over the Mediterranean Sea.

Afterwards, three SL-type SDS episodes were identified on the 26th May, the 7th June 2018 and the 16th March 2019 (Appendix 3), when the air masses originated from the Sahara region and circulated over the Levant region (Figure 10). During these episodes, the back trajectories arriving at 100 m and 500 m originated from over the Mediterranean Sea and circulated over the western parts of Syria, while the trajectories arriving at 1500 m circulated originated from the Sahara region and circulated over Syria, Iraq, and Jordan (i.e. Levant). On the 26th May, the PM_{10} concentration was 108.1 µg/m^3 and $PM_{2.5}$ was 96.5 µg/m^3, on the 7th June PM_{10} was 126.7 µg/m^3 and $PM_{2.5}$ was 127.1 µg/m^3, while on the 16th March 2019 the PM_{10} concentration was 192.6 µg/m^3 but $PM_{2.5}$ mass concentration was not recorded. The cases when $PM_{2.5}$ mass concentration was larger than PM_{10} has been explained in section 3.2.

The SDS episodes were observed to be most intensive during the autumn and winter in 2018, and during the spring in 2019 (Appendix 3). These episodes were identified as the SLA-type SDS (Figure 11). The back trajectories analysis at all the arrival heights confirmed the origin of these SDS to be from the three regions dust sources: Sahara, Arabian Peninsula, and Levant. The PM_{10}

concentration was in the range 87.6–187.3 μg/m^3 and $PM_{2.5}$ was between 51 and 188.9 μg/m^3 during such SDS episodes. Intensive SLA-type episodes were observed during several weeks in October 2018 (Figure 9), with PM_{10} concentrations being higher than 100 μg/m^3 and one measurement reaching 187.3 μg/m^3. The highest $PM_{2.5}$ mass concentration was 188.9 μg/m^3, which was again higher than the recorded highest PM_{10} value within this type of dust episode.

Notice that S-type and SL-type episodes occurred during the summer, where wind speed was observed higher than that in other seasons, and the soil surface was drier. Therefore, the dust particles would have greater chance to be transported over longer distances. These phenomena indicate that some SDS episodes can be lifted to the upper atmosphere while being transported from their source region to the receptor region, where they settle down. The SLA-type episodes occurred during the Autumn, winter and spring, and they recorded higher PM_{10} concentrations than the S-type and SL-type episodes, which occurred in the summer. Furthermore, SLA-type episodes transported dust at any arrival height and the back trajectories crossed over a larger spatial extent than that for the S-type and SL-type episodes.

In comparison to the SDS days, the PM_{10} concentrations lower than 50 μg/m^3 occurred during rainy days or were associated with air masses originating and crossing over the Mediterranean Sea and the eastern part of Europe (Appendix 3, Figure 9, Figure 12). In the European continent, the dust content is relatively lower than that in Sahara, Arabian Peninsula and Levant regions.

Some scientific papers have reported Sahara SDS crossing over the Mediterranean Sea. Riccio et al. (2007) showed that the air mass transported from the African continent was a significant source of mineral dust for western, central and eastern Mediterranean Sea. The heat waves during summertime induced strong convective disturbances, which lifted the dust particles to form suspension/intensive cyclones causing high PM_{10} concentrations to Tunisia, Libya and Algeria. Based on the HYSPLIT4 model, the dust episodes mostly originated from Sahara Desert during 1995–2004. Solomos et al. (2018) analyzed a record-breaking dust episode observed in Crete on the 22nd March 2018 that the 24h mean PM_{10} concentration were 206, 850, and 1125 μg/m^3 in Chania, Finokalia, and Heraklion; respectively. This intense dust episode was a result of a dust plume travelling at low altitudes (0.5–3 km) along the warm conveyor belt preceding the depression cold front, which originated by a polar vortex weakening and the meridional transport of a polar air mass at the upper tropospheric layer resulted in a strong jet streak over north Africa and Central Mediterranean. Therefore, cyclogenesis occurred at the Gulf of Sirte in Libya resulting in strong winds over the north-east parts of Libya that enhanced dust particle emissions. Gkikas et al. (2018) focused on the direct radiative effects of 20 intense and widespread dust outbreaks originated in North Africa and affected the Mediterranean basin during March 2000–February 2013. More studies found out that the dust transport in the Middle East and North Africa (MENA) region is transported from west to east (e.g. Alam et al. 2014; Nabavi et al. 2016; Duchi et al. 2016; Khaniabadi et al. 2017; Yassin et al. 2018; Querol et al. 2019).

These observations are consistent with the observation in Jordan in that most of the SDS originated mainly from North Africa and were transported to the Middle East after crossing/circulating over the Arabian Peninsula and the Levant. Nevertheless, some episodes started within the Levant and the southern region of the Arabian Peninsula.

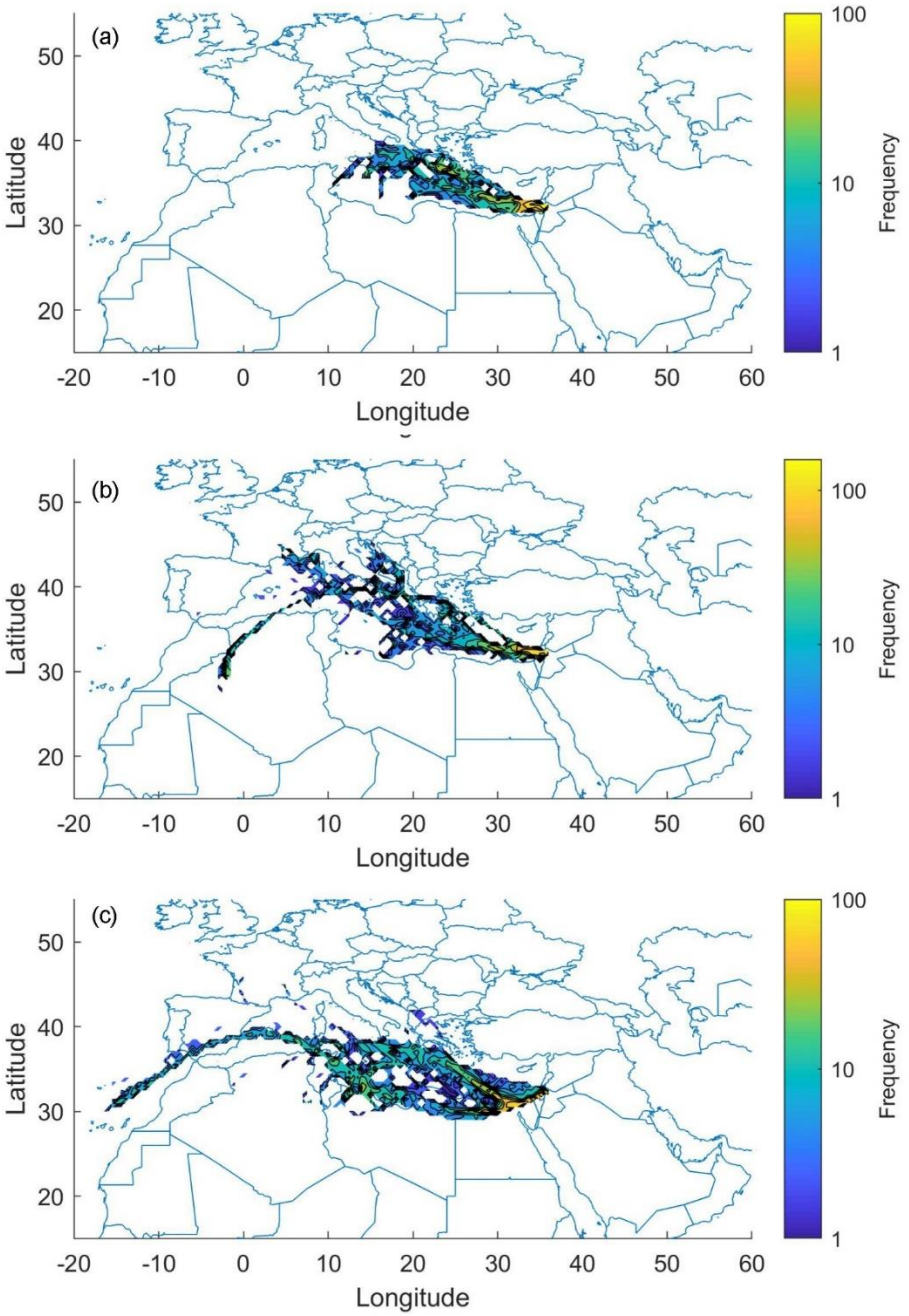

Figure 9. Back trajectories (96 hours) crossing maps during S-type SDS-episodes (indicated on Figure 6) at arrival heights (a) 100 meters, (b) 500 meters, and (c) 1500 meters. The arrival location was the campus of the University of Jordan, Amman, Jordan. These maps were generated from the hourly back trajectories during the sampling dates (+ following day).

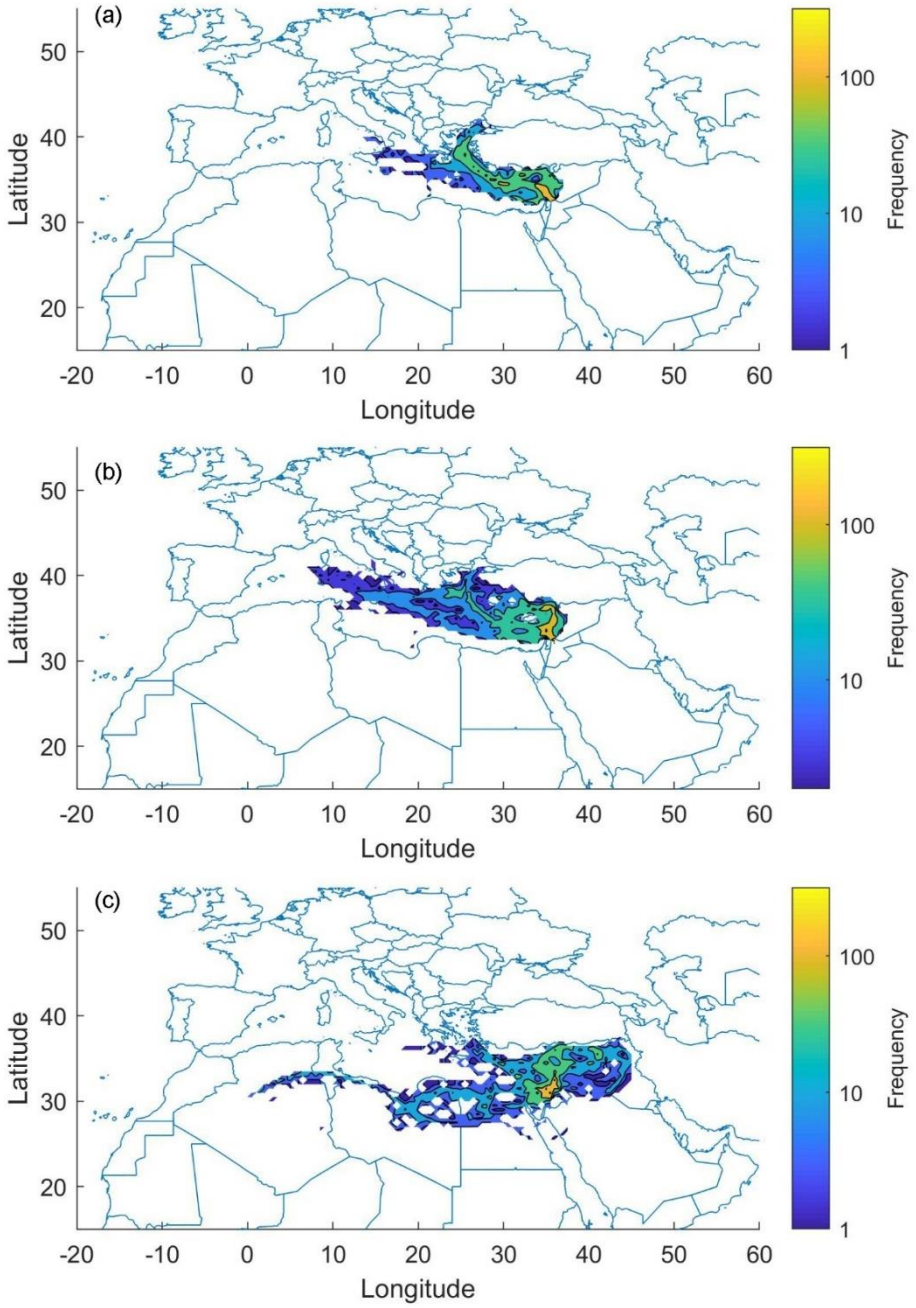

Figure 10. Back trajectories (96 hours) crossing maps during SL-type SDS-episodes (indicated on Figure 6) at arrival heights (a) 100 meters, (b) 500 meters, and (c) 1500 meters. The arrival location was the campus of the University of Jordan, Amman, Jordan. These maps were generated from the hourly back trajectories during the sampling dates (+ following day).

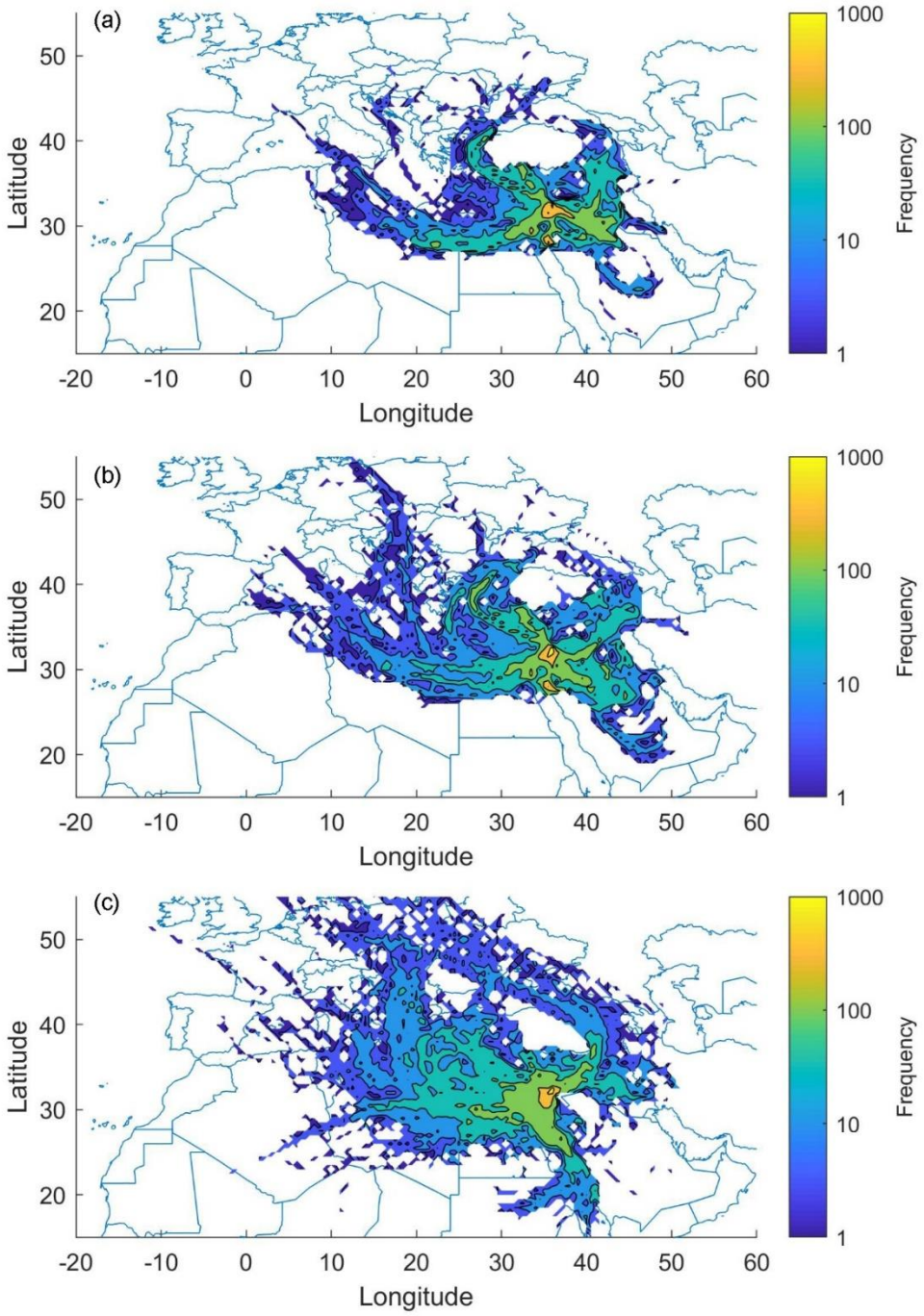

Figure 11. Back trajectories (96 hours) crossing maps during SLA-type SDS-episodes (indicated on Figure 6) at arrival heights (a) 100 meters, (b) 500 meters, and (c) 1500 meters. The arrival location was the campus of the University of Jordan, Amman, Jordan. These maps were generated from the hourly back trajectories during the sampling dates (+ following day).

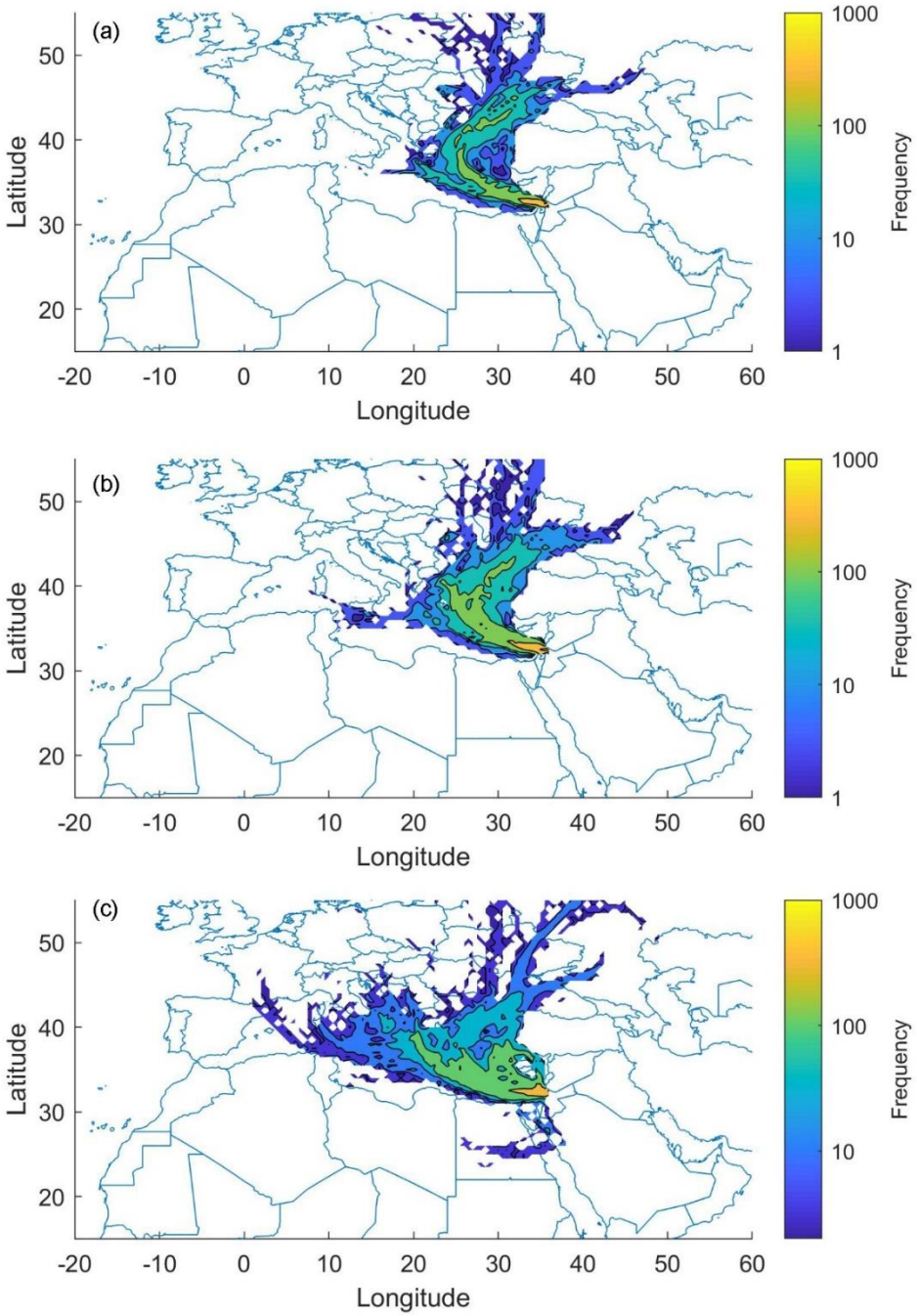

Figure 12. Back trajectories (96 hours) crossing maps during low PM_{10} concentrations (indicated on Figure 6) at arrival heights (a) 100 meters, (b) 500 meters, and (c) 1500 meters. The arrival location was the campus of the University of Jordan, Amman, Jordan. These maps were generated from the hourly back trajectories during the sampling dates (+ following day).

4. Conclusions

Air quality issues related to sand and dust storms (SDS) in the Middle East and North Africa (MENA) are a critical issue that require more attention, because the frequency and the intensity of SDS episodes has increased recently due to escalating climate change impacts and increasing anthropogenic emissions in the region. In this work, the particulate matter ($PM_{2.5}$ and PM_{10}) mass concentrations were measured and investigated during May 2018–March 2019 in the urban atmosphere of Amman, Jordan. The methods included aerosol sampling using high-volume samplers and gravimetric analyses combined with air mass back trajectories. The limitation of the measurement is that the sampling was one 24-hour sample every 6 days, and it is recommended to perform the sampling with higher time resolution (one 24-hour sample per day).

The PM_{10} mass concentration was measured to be in the range of 20-192.6 μg/m^3. The springtime measurements (61.9 – 192.6 μg/m^3) were higher than the records in 2017 (3.7 – 126.4 μg/m^3), suggesting an increasing trend of SDS episodes. The $PM_{2.5}$ / PM_{10} ratio was 0.76±0.2, which means that about 76.5% of the PM_{10} was within the fine fraction. The influence of sampling artefacts resulting in $PM_{2.5}$ / PM_{10} ratios > 100% on a few sampling dates, probably linked to the volatilization of NH_4Cl from filters, requires investigation in the future work.

According to the Jordanian Air Quality standards (JS 1140, 2006), the observed PM_{10} annual mean value was below its limit value but that of the $PM_{2.5}$ was three times higher than its limit value. However, both exceeded the World Health Organization (WHO) air quality guidelines. According to the WHO global ambient air quality database during 2008–2016, the annual mean PM_{10} concentrations in Jordan were lower than what was reported for other cities in the Middle East but were higher when compared to other Mediterranean cities.

During the measurement period, Jordan was affected by SDS episodes for 14 days. The source origins of these dust outbreaks were traced back to North Africa, the Levant, and the Arabian Peninsula, containing both local and regional dust transportation. During these SDS episodes, the 24-hour PM_{10} concentrations was ranged between 108.1 μg/m^3 and 192.6 μg/m^3.

Acknowledgement

This research was funded by the Deanship of Academic Research (DAR, project number 2015) at the University of Jordan. This research was part of a close collaboration between the University of Jordan, Institute of Environmental Assessment and Water Research (IDAEA-CSIC), and the Institute for Atmospheric and Earth System Research (INAR / Physics, University of Helsinki) via the Academy of Finland Center of Excellence (project No. 272041), ERA-PLANET (www.era-planet.eu), trans-national project SMURBS (www.smurbs.eu, grant agreement n. 689443 funded under the EU Horizon 2020 Framework Programme and Academy of Finland via the Center of Excellence in Atmospheric sciences and NanoBioMass (project number 1307537). The eCOST action (inDUST, project number CA16202) is acknowledged for supporting this research via the Short-Term Scientific Mission (STSM) mobility grant.

I would like to thank INAR (University of Helsinki), IDAEA-CSIC (Spanish Research Council), and Department of Physics (University of Jordan) for providing the project to complete the air quality research and the thesis work. My supervisor Prof. Tareq Hussein has provided great help on getting in touch with this project and the guidance of the paperwork, he is also with great patience for any question I had. Prof. Mar Viana from IDAEA-CSIC had helped with the laboratory work and she provided opportunities for me to get familiar with the sample treatment process. Together with Prof. Mar Viana, Rebeca Vázquez and Cristina Reche from IDAEA-CSIC also put invaluable assistance in comprehending the laboratory work on the air sample filters treatment.

References

1. Abdullah Bin Abdulwahed, Jadunandan Dash & Gareth Roberts (2019) An evaluation of satellite dust-detection algorithms in the Middle East region, *International Journal of Remote Sensing*, 40:4, 1331-1356
2. Ahmad Taheri, Pourya Aliasghari, Vahid Hossein (2019), Black carbon and PM2.5 monitoring campaign on the roadside and residential urban background sites in the city of Tehran, *Atmospheric Environment*, Volume 218, 116928, ISSN 1352-2310
3. Aitken, J. (1880). On Dusts, Fogs and Clouds, Nature Feb. 384-385.
4. Alam, K., Trautmann, T., Blaschke, T., & Subhan, F. (2014). Changes in aerosol optical properties due to dust storms in the Middle East and Southwest Asia. *Remote sensing of environment*, *143*, 216-227.
5. d'Almeida, G. A., & Schütz, L. (1983). Number, mass and volume distributions of mineral aerosol and soils of the Sahara. *Journal of Climate and Applied Meteorology*, *22*(2), 233-243.
6. Alonso-Pérez, S., Cuevas, E., & Querol, X. (2011). Objective identification of synoptic meteorological patterns favouring African dust intrusions into the marine boundary layer of the subtropical eastern north Atlantic region. *Meteorology and Atmospheric Physics*, *113*(3-4), 109.
7. Amarloei, Ali & Fazlzadeh, Mehdi & Jonidi jafari, Ahmad & Zarei, Ahmad & Mazloomi, Sajad. (2019). Particulate matter and bioaerosols during Middle East dust storms events in Ilam, Iran. Microchemical Journal. 152. 104280. 10.1016/j.microc.2019.104280.
8. Amiraslani, F., & Dragovich, D. (2011). Combating desertification in Iran over the last 50 years: an overview of changing approaches. *Journal of Environmental Management*, *92*(1), 1-13.
9. Apte, J. S., Marshall, J. D., Cohen, A. J., & Brauer, M. (2015). Addressing global mortality from ambient PM2. 5. *Environmental science & technology*, *49*(13), 8057-8066.
10. Ayman A. Al-Hasaan, Thomas F. Dann & Paul F. Brunet. (2012), 'Air Pollution Monitoring in Amman, Jordan', Journal of the Air & Waste Management Association, 42:6, 814-816
11. Bagnold, Ralph Alger (1941). *The Physics of Blown Sand and Desert Dunes*. 265 pages. London: Methuen.
12. Cao, H., Liu, J., Wang, G., Yang, G., & Luo, L. (2015). Identification of sand and dust storm source areas in Iran. Journal of Arid Land, 7(5), 567-578.
13. Cohen, Aaron. Anderson, H & Ostro, Bart & Pandey, Kiran & Krzyzanowski, Michal & Künzli, Nino & Gutschmidt, Kersten & Pope, C. & Romieu, Isabelle & Samet, Jonathan & Smith, Kirk. (2005). 'The Global Burden of Disease Due to Outdoor Air Pollution'. Journal of toxicology and environmental health. Part A. 68. 1-7.
14. Doronzo, D. M., Khalaf, E. A., Dellino, P., de Tullio, M. D., Dioguardi, F., Gurioli, L., ... & Sulpizio, R. (2015). Local impact of dust storms around a suburban building in arid and semi-arid regions: numerical simulation examples from Dubai and Riyadh, Arabian Peninsula. *Arabian Journal of Geosciences*, *8*(9), 7359-7369.
15. Draxler, R. R., & Hess, G. D. (1997). Description of the HYSPLIT4 modeling system. NOAA Tech. Mem. ERL ARL-224.

16. Draxler, R. R., & Rolph, G. D. (2012). HYSPLIT (HYbrid Single-Particle Lagrangian Integrated Trajectory), NOAA Air Resources Laboratory, Silver Spring, USA.
17. Duchi, R., Cristofanelli, P., Landi, T. C., Arduini, J., Bonafe, U., Bourcier, L., ... & Bonasoni, P. (2016). Long-term (2002–2012) investigation of Saharan dust transport events at Mt. Cimone GAW global station, Italy (2165 m asl). *Elem Sci Anth*, *4*.
18. Evan, A. T., Flamant, C., Gaetani, M., & Guichard, F. (2016). The past, present and future of African dust. Nature, 531(7595), 493-495.
19. Gherboudj, I., Beegum, S. N., & Ghedira, H. (2017). Identifying natural dust source regions over the Middle-East and North-Africa: Estimation of dust emission potential. Earth-Science Reviews, 165, 342-355.
20. Gillette, D., & Walker, T. R. (1977). Characteristics of airborne particles produced by wind erosion of sandy soil, high plains of West Texas. *Soil Sci.,* 123: 97—110.
21. Givati, A., & Rosenfeld, D. (2007). Possible impacts of anthropogenic aerosols on water resources of the Jordan River and the Sea of Galilee. *Water Resources Research*, *43*(10).
22. Gkikas, A., Obiso, V., Pérez García-Pando, C., Jorba, O., Hatzianastassiou, N., Vendrell, L., ... & Baldasano Recio, J. M. (2018). Direct radiative effects during intense Mediterranean desert dust outbreaks. *Atmospheric Chemistry and Physics*, *2018*(18), 8757-8787.
23. Goudie, A. S. (2009). Dust storms: Recent developments. Journal of environmental management, 90(1), 89-94.
24. Hamad, Samera. (2015). Source apportionment of PM2.5 carbonaceous aerosol in Baghdad, Iraq. Atmospheric Research. 156. 80-90. 10.1016/j.atmosres.2014.12.017.
25. Hamidi, M., Kavianpour, M. R., & Shao, Y. (2013). Synoptic analysis of dust storms in the Middle East. *Asia-Pacific Journal of Atmospheric Sciences*, *49*(3), 279-286.
26. Harrison, R. M., & Pio, C. A. (1983). An investigation of the atmospheric HNO3-NH3-NH4NO3 equilibrium relationship in a cool, humid climate. Tellus B: Chemical and Physical Meteorology, 35(2), 155-159.
27. Harrison, R. M., & Kitto, A. M. (1990). Field intercomparison of filter pack and denuder sampling methods for reactive gaseous and particulate pollutants. Atmospheric Environment. Part A. General Topics, 24(10), 2633-2640.
28. Heo, Jongbae & Wu, Bo & Abdeen, Ziad & Qasrawi, Radwan & Sarnat, Jeremy & Sharf, Geula & Shpund, Kobby & Schauer, James. (2017). Source apportionments of ambient fine particulate matter in Israeli, Jordanian, and Palestinian cities. Environmental Pollution. 225. 1-11. 10.1016/j.envpol.2017.01.081.
29. Hinds, W.C. (1999) Aerosol Technology, Properties, Behaviour, and Measurement of Airborne Particles. John Wiley & Sons Inc., New York.
30. Hoek, G., Krishnan, R. M., Beelen, R., Peters, A., Ostro, B., Brunekreef, B., & Kaufman, J. D. (2013). Long-term air pollution exposure and cardio-respiratory mortality: a review. *Environmental health*, *12*(1), 43.
31. Hussein, T., & Betar, A. (2017). Size-fractionated number and mass concentrations in the urban background atmosphere during spring 2014 in Amman–Jordan. *Jordan Journal of Physics*, Volume 10, Number 1, 2017. pp. 49-58

32. Hussein, T., Juwhari, H., Al Kuisi, M., Alkattan, H., Lahlouh, B., & Al-Hunaiti, A. (2018). Accumulation and coarse mode aerosol concentrations and carbonaceous contents in the urban background atmosphere in Amman, Jordan. *Arabian Journal of Geosciences*, *11*(20), 617.
33. Hussein, T., Dada, L., Hakala, S., Petäjä, T., & Kulmala, M. (2019). Urban Aerosol Particle Size Characterization in Eastern Mediterranean Conditions. *Atmosphere*, *10*(11), 710.
34. IPCC (2007) Summary for policymakers in climate change: the physical science basis. Contribution of working group I to the fourth assessment report of the intergovernmental panel on climate change. *Cambridge University Press*, Cambridge, pp 1–18
35. Jeanne, R. L. (Ed.). (2019). Interindividual behavioral variability in social insects. CRC Press.
36. Jish Prakash, P., Stenchikov, G. L., Kalenderski, S., Osipov, S., & Bangalath, H. K. (2015). The impact of dust storms on the Arabian Peninsula and the Red Sea. *Atmospheric Chemistry and Physics*. 15. 199-222. 10.5194/acp-15-199-2015.
37. Jordanian Ambient Air Quality Standards (JS-1140/2006).
38. Keramat, A., Marivani, B., & Samsami, M. (2011). Climatic change, drought and dust crisis in Iran. *World Academy of Science, Engineering and Technology*, *6*, 10-13.
39. Khaniabadi, Y. O., Daryanoosh, S. M., Amrane, A., Polosa, R., Hopke, P. K., Goudarzi, G., ... & Armin, H. (2017). Impact of Middle Eastern Dust storms on human health. *Atmospheric pollution research*, *8*(4), 606-613.
40. Kok, J. F., Parteli, E. J., Michaels, T. I., & Karam, D. B. (2012). The physics of wind-blown sand and dust. Reports on progress in Physics, 75(10), 106901.
41. Kutiel, H. & Furman, H. (2003). Dust Storms in the Middle East: Sources of Origin and their Temporal Characteristics, *Indoor and Built Environment*, vol. 12, no. 6, pp. 419-426.
42. Latif, M. T., Othman, M., Idris, N., Juneng, L., Abdullah, A. M., Hamzah, W. P., ... & Sahani, M. (2018). Impact of regional haze towards air quality in Malaysia: a review. *Atmospheric Environment*, *177*, 28-44.
43. Maring, H., Savoie, D. L., Izaguirre, M. A., Custals, L., & Reid, J. S. (2003). Mineral dust aerosol size distribution change during atmospheric transport. *Journal of Geophysical Research: Atmospheres*, *108*(D19).
44. Mbengue, S., Serfozo, N., Schwarz, J., Ziková, N., Šmejkalová, A. H., & Holoubek, I. (2020). Characterization of Equivalent Black Carbon at a regional background site in Central Europe: Variability and source apportionment☆. *Environmental Pollution*, *260*, 113771.
45. MENCUCCINI, M., AND J. GRACE. (1995). Climate influences the leaf area/sapwood area ratio in Scots pine. *Tree Physiology* 15: 1-10.
46. Middleton, N. J. (1986a). Dust storms in the Middle East. Journal of Arid Environments, 10(2), 83-96.
47. Middleton, N. J. (1986b). A geography of dust storms in South-west Asia. Journal of Climatology, 6(2), 183-196.
48. Middleton, N., & Kang, U. (2017). Sand and dust storms: impact mitigation. *Sustainability*, *9*(6), 1053.

49. Miller, R.L., G.A. Schmidt, and D.T. Shindell. (2006). Forced annular variations in the 20th century Intergovernmental Panel on Climate Change Fourth Assessment Report models. *J. Geophys. Res.*, **111**, D18101, doi:10.1029/2005JD006323.
50. Morales-Baquero, R., Pulido-Villena, E., Romera, O., Ortega-Retuerta, E., Conde-Porcuna, J. M., Pérez-Martínez, C., & Reche, I. (2006). Significance of atmospheric deposition to freshwater ecosystems in the southern Iberian Peninsula. *Limnetica, 25(1-2),* 171-180.
51. Myriam Ababsa (2006). 'Atlas of Jordan: History, Territories and Society'. Chapter ten - Jordan Mega Projects for Water, Energy and Transportation, p. 448-449
52. Nabavi, S. O., Haimberger, L., & Samimi, C. (2016). Climatology of dust distribution over West Asia from homogenized remote sensing data. *Aeolian Research, 21*, 93-107.
53. Natsagdorj, L., D. Jugder, and Y. S. Chung (2003), Analysis of dust storms observed in Mongolia during 1937– 1999, Atmos. Environ., 37, 1401– 1411
54. Notaro, M., Yu, Y., & Kalashnikova, O. V. (2015). Regime shift in Arabian dust activity, triggered by persistent Fertile Crescent drought. *Journal of Geophysical Research: Atmospheres, 120(19),* 10-229.
55. Nidal A. Hadadin and Zeyad S. Tarawneh. (2007). Environmental Issues in Jordan, Solutions and Recommendations. *American Journal of Environmental Sciences* 3 (1): 30-36
56. Pope 3rd, C. A., Bates, D. V., & Raizenne, M. E. (1995). Health effects of particulate air pollution: time for reassessment?. *Environmental health perspectives*, *103*(5), 472-480.
57. Pope iii, C. A., Burnett, R. T., Thun, M. J., Calle, E. E., Krewski, D., Ito, K., & Thurston, G. D. (2002). Lung cancer, cardiopulmonary mortality, and long-term exposure to fine particulate air pollution. *Jama*, *287*(9), 1132-1141.
58. Pope, C.A., III & Dockery, D.W. (2006), "Health effects of fine particulate air pollution: Lines that connect", *Journal of the Air and Waste Management Association*, vol. 56, no. 6, pp. 709-742.
59. Prospero, J. M., Ginoux, P., Torres, O., Nicholson, S. E., & Gill, T. E. (2002). Environmental characterization of global sources of atmospheric soil dust identified with the Nimbus 7 Total Ozone Mapping Spectrometer (TOMS) absorbing aerosol product. Reviews of geophysics, 40(1), 2-1.
60. Putaud, J. P., Van Dingenen, R., Alastuey, A., Bauer, H., Birmili, W., Cyrys, J., ... & Harrison, R. M. (2010). A European aerosol phenomenology–3: Physical and chemical characteristics of particulate matter from 60 rural, urban, and kerbside sites across Europe. *Atmospheric Environment*, *44*(10), 1308-1320.
61. Querol, X., Alastuey, A., Ruiz, C. R., Artiñano, B., Hansson, H. C., Harrison, R. M., ... & Straehl, P. (2004). Speciation and origin of PM10 and PM2. 5 in selected European cities. *Atmospheric Environment*, *38*(38), 6547-6555.
62. Querol, X., Tobías, A., Pérez, N., Karanasiou, A., Amato, F., Stafoggia, M., ... & Mudu, P. (2019). Monitoring the impact of desert dust outbreaks for air quality for health studies. *Environment international*, *130*, 104867.
63. Rashki, A., Arjmand, M., & Kaskaoutis, D. G. (2017). Assessment of dust activity and dust-plume pathways over Jazmurian Basin, southeast Iran. *Aeolian Research*, *24*, 145-160.

64. Rezazadeh, M., Irannejad, P., & Shao, Y. (2013). Climatology of the Middle East dust events. *Aeolian Research, 10*, 103-109.
65. Riccio, A., Giunta, G., & Chianese, E. (2007). The application of a trajectory classification procedure to interpret air pollution measurements in the urban area of Naples (Southern Italy). *Science of the Total Environment, 376*(1-3), 198-214.
66. Saeifar, M.H. & Alijani, B. (2019). Detection of Dust Storm Origins in the Middle East by Remotely Sensed Data. *Journal of the Indian Society of Remote Sensing, vol. 47*, no. 11, pp. 1883-1893.
67. Satheesh, S. K., Deepshikha, S., & Srinivasan, J. (2006). Impact of dust aerosols on Earth–atmosphere clear-sky albedo and its short wave radiative forcing over African and Arabian regions. *International Journal of Remote Sensing, 27(8),* 1691-1706.
68. Seinfeld, J.H. and Pandis, S.N. (2006). 'From air pollution to climate change', Atmospheric chemistry and physics second ed. John Wiley & Sons, Inc., New Jersey, USA.
69. Shao, Y., Raupach, M. R., & Findlater, P. A. (1993). Effect of saltation bombardment on the entrainment of dust by wind. Journal of Geophysical Research: Atmospheres, 98(D7), 12719-12726.
70. Solomos, S., Kalivitis, N., Mihalopoulos, N., Amiridis, V., Kouvarakis, G., Gkikas, A., ... & Pradhan, Y. (2018). From tropospheric folding to Khamsin and Foehn winds: how atmospheric dynamics advanced a record-breaking dust episode in Crete. *Atmosphere*, *9*(7), 240.
71. Stein, A. F., Draxler, R. R., Rolph, G. D., Stunder, B. J., Cohen, M. D., & Ngan, F. (2015). NOAA's HYSPLIT atmospheric transport and dispersion modeling system. *Bulletin of the American Meteorological Society*, *96*(12), 2059-2077.
72. Swann Jr, W. B., Gómez, A., Huici, C., Morales, J., & Hixon, J. G. (2010). Identity fusion and self-sacrifice: arousal as a catalyst of pro-group fighting, dying, and helping behavior. *Journal of personality and social psychology*, *99*(5), 824.
73. United Nations Convention to Combat Desertification (Secretariat), 'GLOBAL ALARM: DUST AND SANDSTORMS FROM THE WORLD'S DRYLANDS', United Nations 2001, p18
74. United Nations Development Programme. (2002). *Human development report 2002: Deepening democracy in a fragmented world*. Oxford University Press.
75. Viana, M., Querol, X., & Alastuey, A. (2006). Chemical characterisation of PM episodes in NE Spain. *Chemosphere*, *62*(6), 947-956.
76. Viana, M., Maenhaut, W., Ten Brink, H. M., Chi, X., Weijers, E., Querol, X., ... & Večeřa, Z. (2007). Comparative analysis of organic and elemental carbon concentrations in carbonaceous aerosols in three European cities. *Atmospheric Environment, 41*(28), 5972-5983.
77. Warneck, P. (1988). Chemistry of the Natural Atmosphere. *INTERNATIONAL GEOPHTSICS SERIES, volume 71*.
78. West, J. J., Smith, S. J., Silva, R. A., Naik, V., Zhang, Y., & Adelman, Z. Co-benefits of global greenhouse gas mitigation for future air quality and human health. *Nat Clim Change. 2013; 3: 885–9.*
79. World Health Organization. 2 May 2018. *Ambient (outdoor) air pollution*. Retrieved from: https://www.who.int/news-room/fact-sheets/detail/ambient-(outdoor)-air-quality-and-health

80. Yassin, M. F., Almutairi, S. K., & Al-Hemoud, A. (2018). Dust storms backward Trajectories' and source identification over Kuwait. *Atmospheric Research*, *212*, 158-171.
81. Zender, C. S., Bian, H., & Newman, D. (2003). Mineral Dust Entrainment and Deposition (DEAD) model: Description and 1990s dust climatology. *Journal of Geophysical Research: Atmospheres*, *108*(D14).
82. Zoljoodi, M., Didevarasl, A., & Saadatabadi, A. R. (2013). Dust events in the western parts of Iran and the relationship with drought expansion over the dust-source areas in Iraq and Syria.
83. Zou, X., Hou, S., Zhang, W., Liu, K., Yu, J., Pang, H., & Liu, Y. (2020). An increase of ammonia emissions from terrestrial ecosystems on the Tibetan Plateau since 1980 deduced from ice core record. Environmental Pollution, 114314.

Appendix 1. Weather conditions monthly minimum, average, standard deviation (SD), and maximum during the measurement period as recorded by the on-site weather station. Legend: *LD* stands for "below detection limit" and *UD* for "over detection limit".

Parameter	Year	Month	Min	Mean	SD	Max
Temperature [°C]	2018	May	11.4	22.7	5.6	37.5
		June	14.8	23.3	4.8	36.8
		July	15.0	24.9	4.4	36.9
		August	17.6	24.0	3.9	32.9
		September	14.0	24.4	4.9	36.2
		October	9.1	20.3	4.7	34.2
		November	7.3	14.0	3.4	25.5
		December	2.1	9.8	2.9	18.9
	2019	January	0.0	7.8	4.0	19.7
		February	1.5	8.5	3.8	23.0
		March	1.5	8.9	4.1	23.2
Pressure [hPa]	2018	May	890.9	897.5	2.4	903.6
		June	890.7	896.0	1.9	900.7
		July	891.1	895.3	1.5	898.9
		August	893.7	896.2	1.2	899.3
		September	894.7	898.9	1.9	903.5
		October	891.9	900.9	2.8	908.7
		November	894.0	900.9	2.9	907.5
		December	892.5	902.0	3.7	908.7
	2019	January	889.5	899.3	3.6	907.5
		February	888.7	900.4	3.8	905.9
		March	890.8	900.3	4.2	909.1
Relative Humidity [%]	2018	May	*LD*	46.3	23.5	*UD*
		June	*LD*	53.7	24.2	*UD*
		July	*LD*	55.2	24.0	*UD*
		August	20.0	65.0	20.3	*UD*
		September	*LD*	54.3	23.4	*UD*
		October	14.0	67.7	23.5	*UD*
		November	29.0	81.3	16.9	*UD*
		December	47.0	88.7	12.5	*UD*
	2019	January	17.0	77.2	19.1	*UD*
		February	22.0	80.6	21.3	*UD*
		March	12.0	84.1	22.7	*UD*
Wind Speed [m/s]	2018	May	*LD*	1.2	1.0	6.5
		June	*LD*	1.8	1.0	6.1
		July	*LD*	2.0	1.1	6.1

	August	*LD*	2.1	1.0	7.1
	September	*LD*	1.4	1.0	5.1
	October	*LD*	1.3	1.0	7.1
	November	*LD*	0.8	0.8	5.4
	December	*LD*	1.2	1.1	7.5
2019	January	*LD*	1.5	1.4	9.2
	February	*LD*	1.3	1.2	7.5
	March	*LD*	1.6	1.3	6.1

Appendix 2. Particulate matter concentrations and overall average temperature and pressure according to the sampling schedule.

Start	End	$PM_{2.5}$ [µg/m^3]	PM_{10} [µg/m^3]	$\frac{PM_{2.5}}{PM_{10}}$	$T_{sampler}$ [^{o}C]	$P_{sampler}$ [hPa]	$T_{station}$ [oC]	$P_{station}$ [hPa]
20-05-2018 13:24	21-05-2018 13:24	52.4	58.3	0.90	25.6	902.7	26.4	899.1
26-05-2018 14:02	27-05-2018 14:02	96.3	107.8	0.89	24.7	900.3	25.5	896.7
01-06-2018 16:15	02-06-2018 16:15	19.1	28.4	0.67	18.8	899.8	19.5	896.3
07-06-2018 10:10	08-06-2018 10:10	127.2	**126.7**	**1.00**	27.4	902.8	32.4	900.6
13-06-2018 11:05	14-06-2018 11:05	20.3	34.3	0.59	21	896	21.7	892.5
19-06-2018 11:00	20-06-2018 10:45	25.7	31.3	0.82	23.3	902.3	25.3	897.8
25-06-2018 12:30	26-06-2018 12:30	24.0	28.9	0.83	23.3	900.8	24.2	897.0
01-07-2018 09:16	02-07-2018 09:16	26.9	34.2	0.79	24.2	900.9	25.1	897.1
07-07-2018 08:59	08-07-2018 08:59	34.6	39.6	0.87	25.2	898.4	25.8	894.5
13-07-2018 09:31	14-07-2018 09:31	32.5	46.5	0.70	22.8	896.3	23.4	892.4
19-07-2018 09:28	20-07-2018 09:28	47.0	57.7	0.82	24.4	898.7	25.1	894.7
25-07-2018 09:26	26-07-2018 09:26	108.5	**120.9**	0.90	28.9	900.8	29.7	896.6
31-07-2018 09:23	01-08-2018 09:23	28.0	33.4	0.84	22.2	900.3	--	--
06-08-2018 09:28	07-08-2018 09:28	26.0	33.3	0.78	23	901.8	23.8	897.9
12-08-2018 09:32	13-08-2018 09:32	35.8	43.0	0.83	24.3	901.3	25.2	897.1
18-08-2018 10:08	19-08-2018 10:08	25.2	34.2	0.74	21.5	898.9	22.3	894.9
24-08-2018 10:43	25-08-2018 10:43	33.7	36.9	0.91	26.8	901	--	--
30-08-2018 08:15	31-08-2018 08:15	35.1	49.2	0.71	25.8	901.4	--	--
05-09-2018 07:51	06-09-2018 07:51	45.5	43.8	**1.04**	24.9	901.3	26.5	896.9
11-09-2018 18:16	12-09-2018 18:16	53.1	53.7	0.99	25.3	903.8	26.4	899.1
23-09-2018 08:17	24-09-2018 08:17	38.3	46.2	0.83	21.9	905.5	23.0	901.5
29-09-2018 09:09	30-09-2018 09:09	59.9	60.9	0.98	27.2	906.3	28.2	901.7
05-10-2018 09:39	06-10-2018 09:39	26.5	30.9	0.86	20	906	20.9	902.0
11-10-2018 08:36	12-10-2018 08:36	60.6	**105.7**	0.57	18.8	903.3	19.6	899.5
17-10-2018 08:37	18-10-2018 08:37	55.2	**158.6**	0.35	18.8	902.8	19.8	898.9
23-10-2018 08:14	24-10-2018 08:14	188.9	**188.3**	**1.00**	24.2	904.2	25.2	899.7
04-11-2018 09:09	05-11-2018 09:09	43.6	58.0	0.75	13.3	900.8	14.0	897.3
10-11-2018 09:07	11-11-2018 09:07	37.3	41.6	0.89	12.7	904.4	13.9	900.7
16-11-2018 10:00	17-11-2018 10:00	21.2	30.7	0.69	10.3	908.1	11.1	904.9
22-11-2018 09:20	23-11-2018 09:20	35.0	47.5	0.74	11.6	902	12.6	898.7
28-11-2018 08:37	29-11-2018 08:37	51.3	**88.3**	0.58	15	904.8	16.2	901.1
04-12-2018 08:52	05-12-2018 08:52	32.7	49.0	0.67	9.4	900.3	10.3	897.0
10-12-2018 09:42	11-12-2018 09:42	27.6	51.8	0.53	9.3	905.4	10.5	902.2
16-12-2018 16:05	17-12-2018 16:05	43.8	**88.5**	0.50	9.8	904.5	10.6	900.9
22-12-2018 08:39	23-12-2018 08:39	29.0	41.1	0.71	7.1	908.6	8.3	905.6
03-01-2019 08:25	04-01-2019 08:25	89.4	**141.9**	0.63	5.2	907.8	6.0	904.9

09-01-2019	13:10	10-01-2019	13:10	24.6	27.5	0.89	3.6	907.8	4.4	904.9
15-01-2019	08:45	16-01-2019	08:45	79.7	**92.6**	0.86	6.5	899.2	7.7	895.9
21-01-2019	08:20	22-01-2019	08:20	56.9	**104.0**	0.55	8.5	902.9	10.0	900.4
27-01-2019	08:15	28-01-2019	08:15	48.6	53.1	0.91	5.3	901.6	10.2	895.0
02-02-2019	07:37	03-02-2019	07:37	23.9	36.6	0.65	7.2	906.7	8.2	903.5
08-02-2019	08:53	09-02-2019	08:53	23.8	54.4	0.44	7.5	901.9	8.4	898.5
14-02-2019	07:54	15-02-2019	07:54	69.2	**111.8**	0.62	6.3	898.6	7.1	895.3
20-02-2019	07:47	21-02-2019	07:47	31.4	38.0	0.83	7.6	896.9	8.6	903.3
26-02-2019	08:04	27-02-2019	08:04	--	**137.7**	--	9.5	896.9	10.2	893.2
28-02-2019	08:40	01-03-2019	08:40	14.9	19.3	0.77	2.5	895	--	--
04-03-2019	08:25	05-03-2019	08:25	37.7	62.2	0.61	9.5	896.9	7.7	899.3
10-03-2019	09:04	11-03-2019	09:04	49.4	53.5	0.92	9.1	907	9.8	903.6

Appendix 3. Sand and Dust Storm (SDS) episodes according to type and observation during the sampling period. The type of SDS is denoted as: Saharan (S); Saharan and Levant (SL); Saharan, Arabian, and Levant (SLA); Saharan, Arabian, Levant, and Ahvaz (SALA). The source region was verified according to the back-trajectory's analysis for crossing maps on the sampling day (+ following day). The date here indicates the start of the sampling day.

SDS Types	Source Region	Dates	PM_{10} [$\mu g/m^3$]
S	Saharan	25-07-2018	120.9
SL	Saharan and Levant	26-05-2018	107.8
		07-06-2018	126.7
		16-03-2018	192.6
SLA	Saharan, Levant, and Arabian	11-10-2018	105.7
		17-10-2018	158.6
		23-10-2018	188.3
		28-11-2018	88.3
		16-12-2018	88.5
		03-01-2019	141.9
		15-01-2019	92.6
		21-01-2019	104.0
		14-02-2019	111.8
		26-02-2019	137.7
CLEAN	Eastern Mediterranean Sea	01-06-2018	28.4
		31-07-2018	33.4
		06-08-2018	33.3
		12-08-2018	43.0
		18-08-2018	34.2
		24-08-2018	36.9
		28-02-2019	19.3

Appendix 4. PM_{10} mass concentration frequencies within the measurement period. The red line stands for the group division border of PM_{10} below and above 70 µg/m^3 due to the natural break of the data.